Proc. of SPIE Vol. 1167, Precision Engineering and Optomechanics, ed. D Vukobratovich (Nov 1989) Copyright SPIE

The chopping secondary mirror for the Kuiper Airborne Observatory

Charles H. Downey, Randal S. Abbott, Phillip I. Arter,
Dale A. Hope, Dan A. Payne, and E.A. Roybal
Ball Aerospace Systems Group
P.O. Box 1062, Boulder, CO 80306

Daniel F. Lester
Department of Astronomy
University of Texas, Austin, TX 78712

James O. McClenahan
NASA/Ames Research Center
Mountain View, CA 94035

ABSTRACT

This paper reports on the design, construction, and implementation of a new chopping secondary mirror system for the Kuiper Airborne Observatory. This observatory facility maintains a 0.91 m diameter telescope in a modified C-141 aircraft at the NASA Ames Research Center. This telescope is routinely used at stratospheric altitudes for astronomical observations at infrared and submillimeter wavelengths that are inaccessible from the ground.

1. INTRODUCTION AND SUMMARY

An infrared optimized telescope uses a chopping secondary mirror to switch the instrument beam back and forth between positions in the sky with a squarewave pattern. This allows synchronous detection of signal from an astronomical source in parts of the spectrum where these observations are strongly background-limited by thermal emission from the telescope and the atmosphere. To most efficiently reject this fluctuating background emission, which has a roughly 1/f spectrum, the highest possible chop frequency is desired. To maximize the spatial dynamic range of the observation, the highest possible chop amplitude is desired. These parameters must be traded off for chopper duty cycle (the fraction of the time that the astronomical source is, in fact, in the focal plane aperture of the instrument). For background-limited measurements of compact astronomical sources, as small a focal plane aperture as possible is used, and this further constrains the duty cycle. In order to be able to make these infrared measurements with high spatial resolution, and to produce a well-defined point source profile for image restoration work, it is further required that the secondary mirror chop with a waveform that is stable over time on a spatial scale that is smaller than other sources of image degradation (such as "seeing" and tracking accuracy).

The secondary mirror assembly, shown in Figure 1, is mounted with a four-legged spider to the telescope's 1 meter diameter head ring. The new hyperbolic secondary mirror is made from a 7.3 inch diameter aluminum blank which has been 70 percent lightweighted to reduce mass, thereby greatly improving its chopping performance. An extensive tradeoff study led us to select a bare diamond turned aluminum mirror, which was lightweighted with a waffle-iron pattern on the back over the other mirror candidates in order to reduce its moment of inertia and still maintain a $\lambda/2$ wave optical figure at the design operating temperature of -40 °C. The mirror, which

weights 1.1 lb, can be chopped with a square wave pattern in any axis at frequencies up to 40 Hz, with transition times of <5 msec and throw angles up to ±23 arcmin (corresponding to ±10 arcmin in the sky).

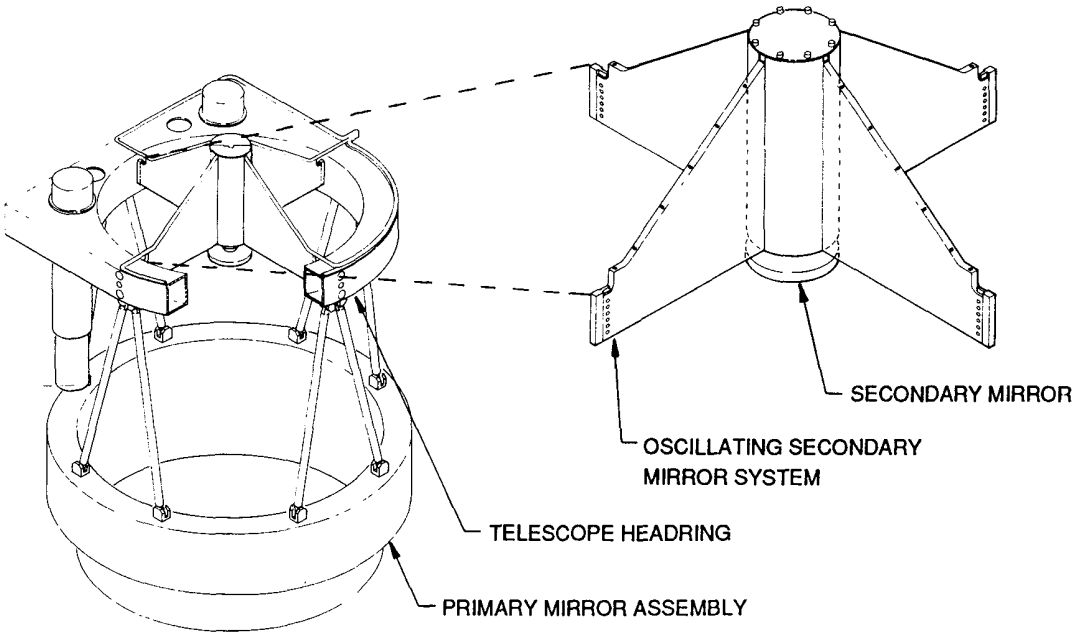

Fig. 1. Kuiper Airborne Observatory Telescope.

The mirror is driven by four electromagnetic actuators located symmetrically on the backside of the mirror. To minimize thermal distortions in the mirror, the high-powered actuator driver coils are mounted to a stationary baseplate. The actuator magnets are attached to a mounting plate, to which the mirror is in turn attached through its obscured central area. This prevents mounting stresses from being introduced into the mirror and allows mirror replacement without disturbing the alignment between the moving and stationary parts of the actuators. In this design no electrical wires cross the gimbal interface, which simplifies maintenance and mirror replacement.

To prevent exciting unwanted structural modes in the supporting spider and telescope structure, the mirror is pivoted about its rotating center of mass through a centrally mounted, two-axis flex pivot gimbal. The entire mirror and chopping assembly can be translated axially to perform focus adjustment.

A state-space controller is used to achieve optimum step and settle performance. This type of control system is straightforward to implement and is very robust against changes in mass and dynamical properties of the chopping mirror system.

The overall electronics is controlled by a 8032-based microprocessor which handles the input and output of all mirror control functions, performs unit conversions for front panel display, and interfaces with other airborne equipment. To prevent exposing any of the electronics to the rigors of the cold environment at 45,000 feet, all electronics, including the position sensing electronics and actuator driver, is located about 25 meters away inside the aircraft cabin.

2. MECHANICAL DESIGN

The mechanical portion of the KAO secondary mirror system consists of the mirror and its associated two-axis gimbal and drive system, as well as a precision focus mechanism. All of these components are suspended with a four-legged spider and are contained within a cylinder which is 7 inches in diameter and 15 inches long.

The mechanical system was designed to achieve high chop rates with the highest possible duty cycle and stability at the angular extremes. Aluminum was used for all structural members to match the existing telescope headring and minimize differential temperature effects. A four-legged spider with four pre-existing attach points to the telescope headring allow for three-axis adjustment (tilt and centering), as well as compressive preload.

The cylindrical housing mounts the focus drive mechanism and transmits the compressive preload forces through linear bearings to the rigid focus shuttle, to which the mirror and drive assembly are attached. Open-loop focus control is accomplished with a dc motor and ballscrew with a range of ±1.3 cm and a resolution of 0.001 cm. Position is sensed by a LVDT and displayed on the front panel in centimeters.

The modular mirror drive assembly shown in Figure 2 consists of a baseplate, actuators, position sensors, and gimballed hub. The drive module can be replaced in about one hour. The moving parts, including the mirror, have a total weight of about 2 lb. The assembly is balanced around its center of mass, eliminating force reactions and the structural modes they excite.

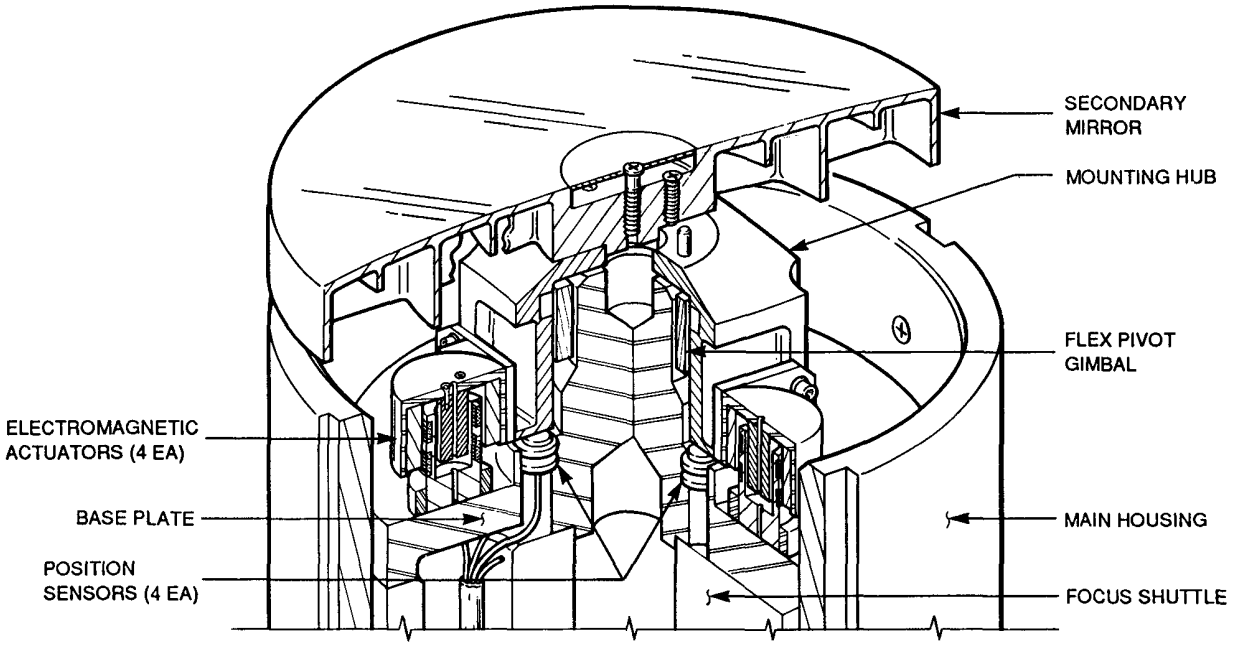

Fig. 2. Mirror drive assembly.

High-performance linear voice coil actuators are used in push-pull fashion to provide the motive force for the mirror. To minimize thermally induced distortions in the mirror from the high-powered actuators, the magnet assemblies are mounted on the

moving portion of the hub assembly and the coils are stationary, wound on eddy current suppressing spools that conduct heat away from the mirror through the baseplate to the large thermal mass of the focus shuttle. A peak force of 20 lb per actuator provides the high acceleration necessary for fast mirror transition times.

The secondary mirror is attached to a central hub which is mounted through an internal gimbal ring to the baseplate post. Standard flexural pivots are used, allowing motion around the two rotational axes while constraining the other four degrees of freedom with very high spring rates.

Mirror position is sensed by magnetic sensors called differential impedance transducers. Four noncontacting, inductance-type sensor coils are mounted in the baseplate and use the back surface of the hub as their target. This type of position sensor has a bandwidth greater than 10 kHz and angular resolution better than 0.1 arcsec. The sensor electronics is remotely located in the control chassis and provides position feedback for the servo control system.

The limit on the speed at which a mirror can be steered is usually dictated by two factors: the angular acceleration capability of the mirror/actuator system and the rigidity of the supporting structure. Our design approach was to maximize both within the technical and dimensional constraints imposed by the KAO facility. Preliminary analysis suggested that, with proper design of the spider/mirror assembly, both actuator force and structural resonances would lead to about the same limitation on control system bandwidth. This turned out to be approximately correct.

The structural rigidity is measured by the natural frequencies of the first pitching and the axial modes of the spider/mirror assembly. These are the modes that couple with the control system and limit its bandwidth. There are numerous low-frequency modes in such systems which do not couple with the control system, since they are not directly excitable by the mirror motion. The pitching modes are, of course, directly excitable by the mirror torque reactions, and the axial mode has been shown by experience at Ball to be excited by any imbalance that exists between the plus and minus driver forces on opposite sides of the mirror. The critical pitching and axial modes can be raised to very high natural frequencies by proper design, thus allowing the necessary high control bandwidth. It was originally estimated that these modes would be about 500 Hz if the design is carefully optimized. It was expected that this would allow the use of a control bandwidth of about 170 Hz. Actually, the minimum resonant frequency turned out to be about 1,040 Hz and easily supports the 170 Hz bandwidth of the control system.

3. MIRROR DESIGN, TEST, AND FABRICATION

The mirror substrate design drivers were weight, optical performance throughout operating temperatures, mirror interchangeability, cost, and schedule. With regard to weight, fabricating the mirror from a low-expansion glass substrate would have introduced several problems in mirror mount design. It is estimated that the weight of a lightweight glass mirror would be 1.5 lb. Beryllium, silicon carbide, and foam-structured aluminum substrates were also considered but rejected because of schedule, cost, or high-technology risk. Other issues such as ruggedness and interchangeability led to the design of an aluminum substrate mirror.

The secondary mirror is a 185.4 cm diameter lightweighted hyperbola with a nominal focal length of 39.4 cm. The substrate material is 0.7 inch thick 5083-0 aluminum.

It is center-mounted on three coplanar pads via three screws and Belleville spring washers to minimize distortions and provide thermal compensation for the difference between the stainless steel mounting screws and aluminum interface. The mirror weight of 1.1 lb was achieved with the lightweighting pattern as shown in the photo in Figure 3. This represents about 70 percent weight relief for a solid mirror having an aspect ratio of about 7:1. The mirror optical surface was diamond turned to final figure. A thin layer of high-purity aluminum and silicon monoxide were applied for a durable broadband spectral performance. Mirror replacement requires less than 30 minutes, and the diamond turned mounting pads on the back side preserve alignment. No optical adjustments are required when mirrors are exchanged.

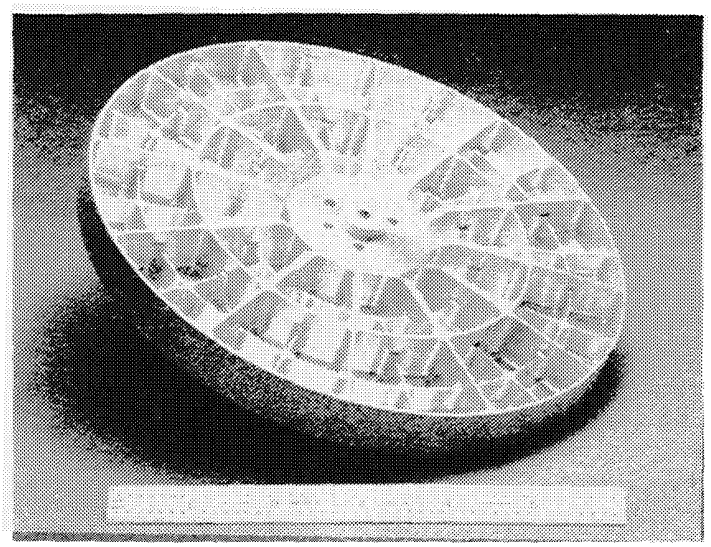

Fig. 3. Back side view of the lightweighted KAO secondary mirror.

It was decided to pursue manufacture of three lightweighted secondary mirrors for final surfacing by three different vendors. Ball provided the weight-relieved substrates with a near fit sphere on the front surface. The three separate optical vendors then diamond turned the reference datum mounting pads and optical surfaces. The flight mirror, which was finished by Optical Filter Corporation, was notably superior to those turned by the other two vendors and was chosen for the remaining flight units. The mirrors were then evaluated for surface roughness, focal length, wavefront error, point spread function, and optomechanical alignment. All the tests were conducted on-axis with fasteners torqued to flight requirements. The data presented here is for the best of three mirrors selected for flight use.

Since the KAO primary mirror was not available for testing the secondary mirrors, a Hindlesphere and a laser unequal path interferometer (LUPI) arrangement was used for optical evaluation as shown in Figure 4. The secondary mirror was aligned to the Hindlesphere LUPI axis, and a measure of the wavefront error at 633 nm was obtained. Because of limitations of the Hindlesphere aperture, the wavefront tests were limited to approximately 90 percent of the secondary clear aperture. First order verification of spot size and focal length was also accomplished with this arrangement using a beam scan device in the optics path. A point source image evaluation was performed with a whitelight parafocal microscope device. This test was to confirm the spot size measurements and evaluate some coherence problems experienced with the beam scan measurement device. The cusps generated during diamond turning create a grating-like surface. This causes spreading of the higher order spatial components

of the coherent PSF. The theoretical spot size derived from the wavefront analysis is in agreement with the white light spot size measurements and the flight data obtained after installation in the observatory.

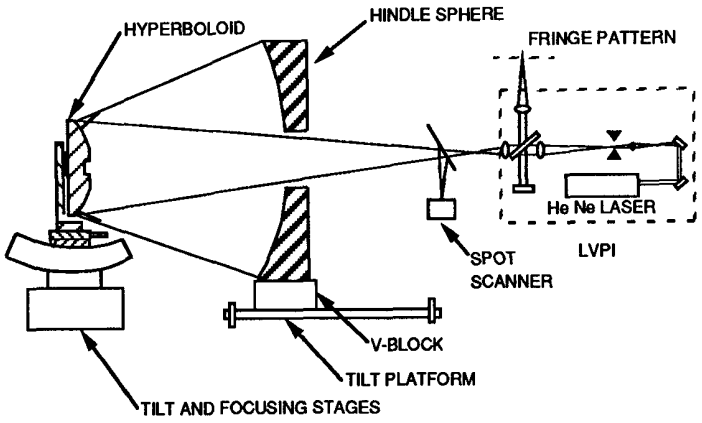

Fig. 4. Mirror test configuration.

Figures 5 and 6 show, respectively, the mirror wavefront interferograms and the calculated point spread function (PSF) obtained through interferogram digitization. This data is for 0.633 nm on axis. The wavefront error is 0.65 waves PV for 90 percent of the clear aperture.

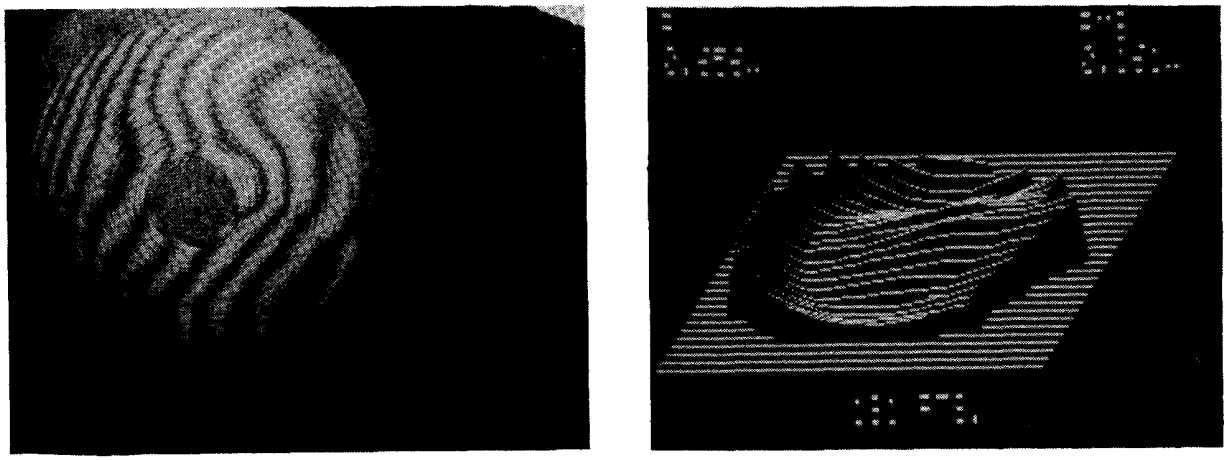

Fig. 5. Wavefront interferograms.

The surface roughness was evaluated by performing a relative test on each of the three mirrors. A relative measure of the diamond turning ripple or surface roughness was obtained by illuminating the mirror with a helium neon laser beam and observing the linear satellite images that occur with coherent illumination. It is possible to measure the relative intensity of the zero order laser beam image to obtain qualitative data; however, after first order testing it was obvious that the mirror supplied by the Optical Filter Corporation had the best optical properties for the other tests and also had the lowest surface scatter. The surface roughness is estimated to be about 80 (A) RMS by visual comparison to measured reference samples.

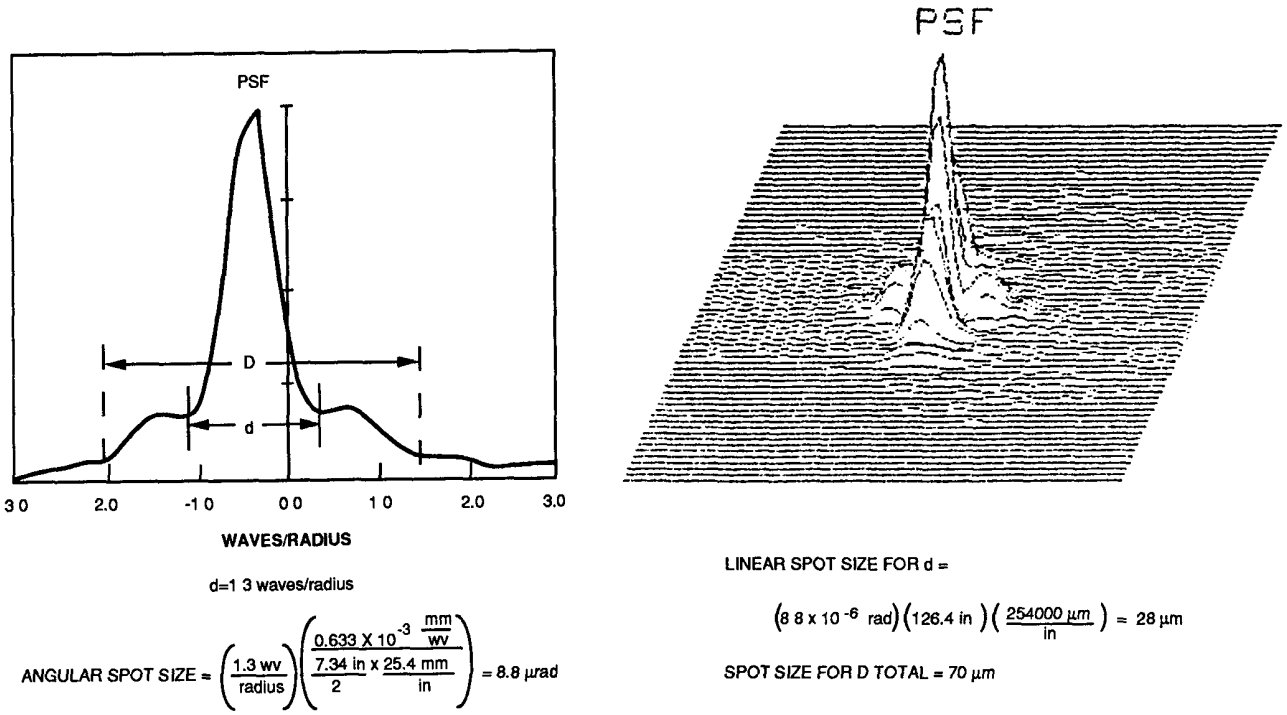

Fig. 6. Calculated point spread functions.

The interferograms presented in Figure 5 represent the hyperboloid in double pass. The PV, RMS numbers have been converted to equivalent surface values. The test setup was a standard Hindle test as shown in Figure 4. The ZYGO ZAPP system was used to analyze the interferograms. The analysis shows the mirror to be 0.65 PV, 0.16 RMS.

The test setup illustrated in Figure 4 was used to measure the surface figure of the hyperboloid. The test configuration is that of a standard Hindle test. The LUPI feeds a spherical wavefront to the convex hyperboloid, which has its short focus coincident with that of the spherical Hindle mirror. The reflection from the hyperboloid is reflected to the sphere and back to the hyperboloid. After a second reflection off the hyperboloid, the light is returned to the LUPI where a fringe pattern is created and recorded. A beamsplitter in front of the LUPI allows the focused spot returning from the mirror to be measured.

The on-axis, cross-sectional, and isometric plots of the PSF shown in Figure 6 were calculated using the WISP software package. The PSF is calculated by doing a Fourier transform analysis on the optical path difference data. The PSF scale is given in the dimensionless waves/radius units. This is converted to real angular spot size by substituting the actual values for wavelength and radius of the diffracting aperture, which in this case is the radius of the hyperboloid (wavelength = 0.6328 μm, radius = 3.67 in.). The calculation shows the angular spot size at the first minimum to be ~9 μrad. The isometric plot shows the PSF to be somewhat asymmetrical, so the average spot size is slightly larger than 9 μrad. In comparison, a diffraction-limited mirror would have yielded a 4.5 μrad image.

During diamond machining of a lightweighted mirror it was found that the structural design of the cored rear side, which produced a weight savings of 70 percent, gave

sufficient rigidity to the mirror to not require the use of any damping compounds. With other thin shell mirrors it has been necessary to fill or coat the rear surfaces with waxes or RTVs or the like to prevent chattering.

The first diamond machining operation was to qualify the rear surface and datum diameters by mounting on the 1.490 diameter counter bore on the convex side. The entire rear reference surfaces were machined all in the same setup. The machining was performed on a two-axis, interferometrically controlled lathe. The part was mounted on an air-bearing spindle on the "Z" slide; the diamond tool was mounted on the "X" slide. Both axes are programmed to follow the cutting path.

The convex hyperboloidal surface was cut while the part was mounted on the reference diameter land (machined in the previous operation) to a fixture held to the machine spindle by vacuum. The fixture mounting surface was, of course, diamond machined first. By mounting an optically flat surface to an optically flat fixture, little, if any, stress was induced.

4. CONTROL SYSTEM

The key performance issue considered in determining the control system architecture for the KAO chopper mirror was the requirement that the control system be capable of tilting the 7.3 inch mirror up to 23 arcmin in 5 msec with negligible overshoot. This performance must be maintained over a wide operating temperature range and for several mirrors with different MOI characteristics.

The requirements were met by combining the desired features of both the state space and the classical approaches into a single control system. In the state space approach, all of the system states (position, rate, acceleration, etc.) are fed back, as opposed to the classical approach where only position and possibly rate are fed back to close the loop. A state-space controller is used to move the system poles to positions on the s-plane such that when the outer position loop is closed around an integrator and gain stage, the poles move to their final desired positions. This results in a system that has no zeros in the forward path to introduce overshoot in the step response and at the same time provides zero steady state error. A block diagram of the analytical model of the combined state-space and classical control system is shown in Figure 7.

Through the addition of an extra state in the state controller and some block diagram manipulation, it was possible to obtain full state feedback characteristics without actually measuring mirror rate, as shown in Figure 8. All other states in the system can be measured directly without additional sensors on the mirror. The position feedback was obtained using differential impedance transducers that provide a voltage output as a function of the mirror angle. Notice in Figure 8 that the position feedback is summed both at the input to the state-space portion of the compensator and to the next stage after the integrator. The acceleration term was obtained by measuring the drive current to the actuators used to drive the mirror and by making the appropriate scale factor adjustments. The additional state, which

is synthetically generated to indirectly measure the rate feedback, completes the list of states required for a full state feedback system.

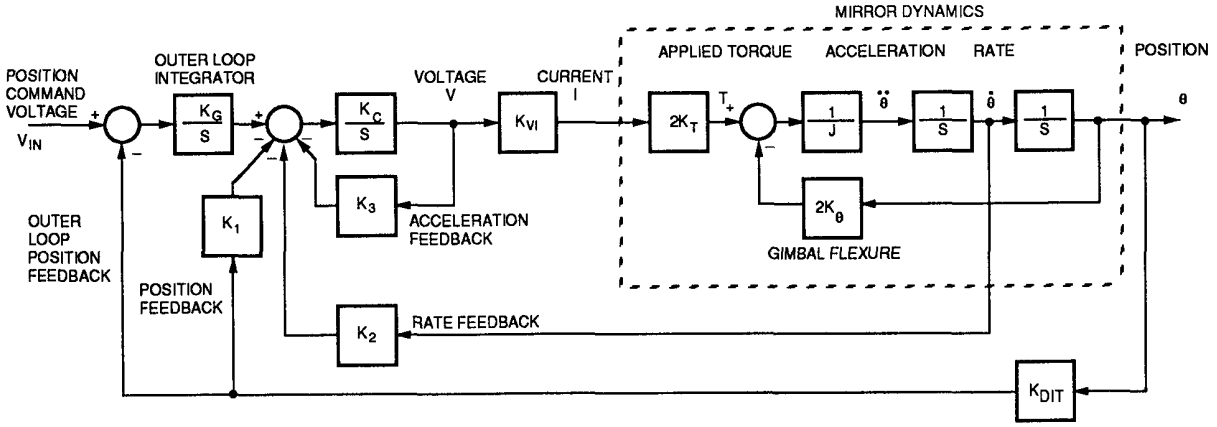

Fig. 7. Single-axis block diagram with full state feedback and outer loop steady state error compensation.

The control system in Figure 8 is not implementable in the form shown; however, with some block diagram manipulation, a configuration that is easily implemented is obtained as shown in Figure 9. In this final form, the control system retains all of the desired features expected for a full state feedback system such as insensitivity to mirror parameter variations, negligible overshoot in response to a step input, and nearly optimal settling time for the given closed-loop bandwidth. With the added outer loop containing the integrator, the requirement for zero steady state error in response to a step input is easily met.

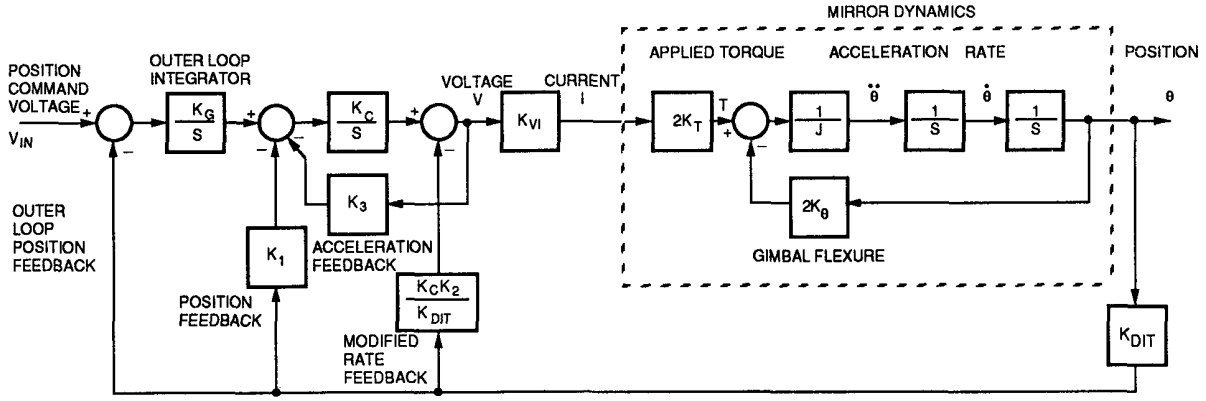

Fig. 8. Single-axis block diagram with modified rate feedback and outer loop steady state error compensation.

Not shown in the block diagrams is an additional feature that was added to the control system to ensure stability at system power up and in the event of actuator driver amplifier saturation. An automatic gain control was added to the control system to lower the outer loop gain if the actuator driver stage starts to saturate. The AFC gain, trigger level, attack time, and decay time were adjusted, as required, to ensure unconditional stability for the control system while still maintaining a clean response to a step input.

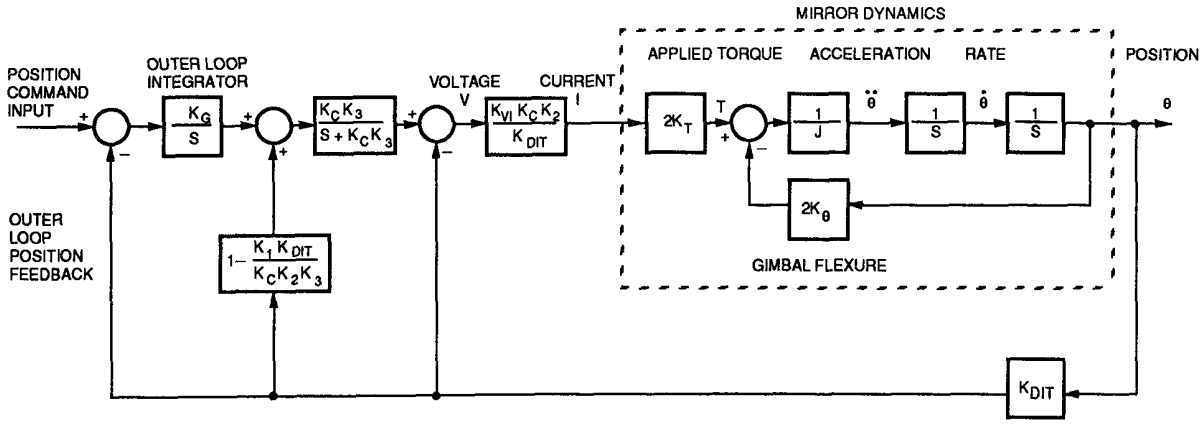

Fig. 9. Single-axis block diagram with modification for implementation and outer loop steady state error compensation.

The frequency response of the closed-loop system was measured while the chopper mirror was installed in the KAO telescope, as shown in Figure 10. Notice the two-pole, slightly overdamped rolloff at 170 Hz and the secondary pole rolloff occurring at 300 Hz. Referring to Figure 10, the only measurable structural resonance occurred at 1040 Hz with an associated zero located at 850 Hz. This structural resonance was effectively compensated with a high Q twin-T active notch with a notch frequency at 950 Hz. The notch was located at 950 Hz not to directly notch the resonance mode, but rather to force the mode poles to move to the left in an arc to intercept the notch zeros. Moving the mode poles in this manner increases the damping ratio.

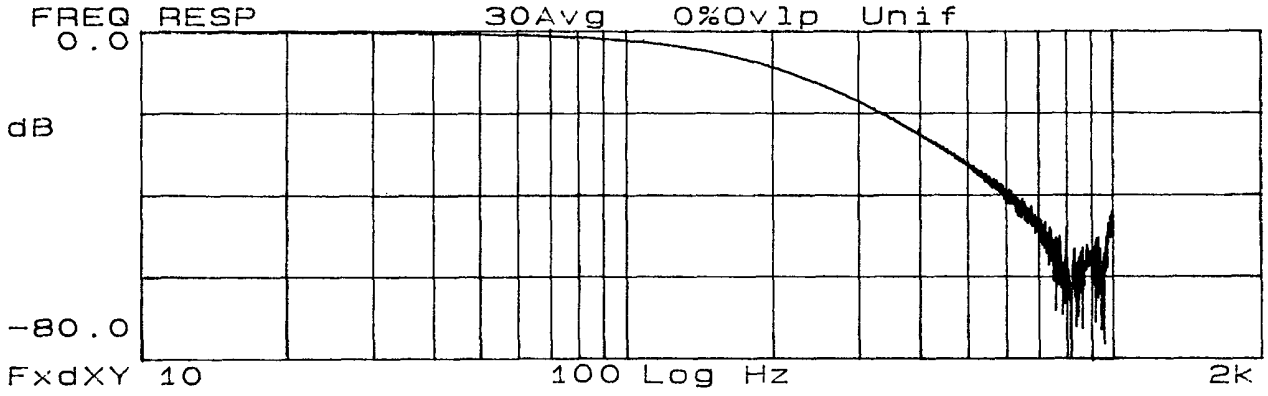

Fig. 10. Closed-loop frequency response.

The step response for a 22 arcmin step command and the corresponding actuator drive current are shown in Figure 11. Notice negligible overshoot and the fast settling time.

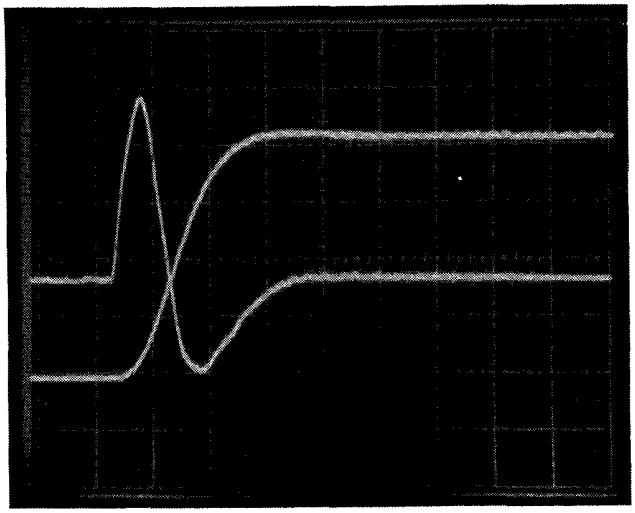

Fig. 11. Actuator drive and mirror position for a 22 arcmin mirror deflection.

5. ELECTRONICS AND SOFTWARE

The electronic circuitry provides a means of inputting signals to the mirror controller, and of monitoring and displaying the actual mirror performance. A microprocessor and its associated software are used to (1) convert the input control parameters which are in polar coordinates to two alternating pairs of voltage levels as X, Y coordinate inputs to the state-space controller boards, and (2) convert the output received from the (X, Y) position sensors that monitor the mirror's position back into polar coordinates for display. The mirror control system described in the previous section is implemented with analog circuitry and does not require any computational assistance from the microprocessor except for the input and display functions identified above.

Input of the control parameters is provided by five sets of front panel switches. The first four sets are binary weighted thumbwheel switches and provide input to the microprocessor. The last (focus) does not input to the processor but to logic circuits that directly drive the focus motor. The front panel controls provided are: chop frequency, chop amplitude, chop angle, offset (of the center point along the chop angle), and focus (mirror position along the central telescope axis).

The signals from the front panel switches (excepting focus) pass through peripheral interface chips which are controlled by the Intel 8032 microprocessor. The processor, supported by UV EPROM and RAM external to the processor chip, passes its output through other peripheral chips to D/A converters whose output goes to the space-state controller boards. The outputs of these boards and the subsequent current drivers drive the actuators that move the mirror. The outputs of the mirror position sensors are monitored by the controller boards for the immediate control of mirror position, and also by the microprocessor by means of an A/D converter. The resulting output of the processor is sent via other peripheral ports to display drivers and LED displays.

The focus control switch has a fast and a slow setting. In its fast setting it provides a dc signal to the logic which controls the 28 volt dc focus motor. In the

slow setting it provides pulses, thus effectively reducing the average dc voltage to the motor and allowing it to run more slowly. The focus position is monitored by the linear variable displacement transformer which provides a dc output signal. This passes through the multiplexed A/D converter to the microprocessor and through a peripheral port to the display.

The electronics system provides external inputs and outputs for external control and monitoring of the mirror as an alternative to using the front panel switches and internal oscillator. Thus, the mirror can be driven externally with any waveforms. An RS 232 interface is also provided for use in possible future control by an external computer.

The software for the 8032 microprocessor is written in C and compiled into 10 K bytes of EPROM. An off-chip RAM is also available for scratch pad operations. The major tasks performed by the software are: (1) accept inputs from the front panel switches, (2) perform conversion to engineering units for all input and output data, (3) perform coordinate rotation from polar to rectangular and back for mirror control and I/O, (4) generate the time base for the mirror chop frequency, and (5) provide output for display of mirror performance.

The software continuously goes through a loop that checks the various inputs to the microprocessor from the front panel switches, the mirror position sensors, and the LVDT. The newest data is then compared to the previous data; if there is no difference, the loop repeats. When a difference is detected, the output data to the mirror and to the displays are recalculated.

The input chop angle entered from the front panel is in polar coordinates referenced to the aircraft. Since it was necessary (for mechanical reasons) to orient the actuators and mirror position sensors at 45 deg to these coordinates (such that a drop in elevation or azimuth requires equal amplitudes for both axes), the first calculating job of the software is to rotate the inputs to the coordinates of the actuators. Next, the software converts the polar coordinates (angle and amplitude) to cartesian coordinates, which is the form necessary to drive the actuators.

The mirror chop frequency can be varied from dc to 40 Hz. The clocking signal for this frequency is generated in software by activating a priority interrupt which is generated when an internal timer and counter signal the mirror to change states. This same scheme is used to generate the time base used to update the chop frequency display.

The outputs from the X, Y position sensors monitoring the mirror position are provided to the processor, and the polar display is derived from these two pairs of numbers representing the end positions of the mirror. By deriving the displayed parameters directly from the actual mirror position, the real mirror behavior can be directly compared to the desired mirror behavior as displayed on the input thumbwheel switches.

6. AIRCRAFT INSTALLATION

After installation in the KAO, the structural resonance at 1040 Hz was found to limit the operation at full bandwidth. Interestingly, the system would ring at high altitude and cold, but not at room temperature. The mirror resonance was identified as the culprit. An attempt to correct the problem using a dampening material on the

back side of the mirror resulted in a partial solution. A notch filter located at about 100 Hz below the resonance solved the problem.

At the initial installation in the aircraft, the system had a tendency toward instability. To assure stable performance, the control system was initially operated with reduced bandwidth, which limited the mirror transition time to about 8 msec.

To analyze the problem, careful gain-phase measurements were made and input to a model of the control system. After some iterations, the model agreed very closely with the hardware performance. The model then allowed us to verify the adequacy of the notch filter mentioned previously and confirmed the necessary changes to the compensation network.

By comparing the results obtained with the model to measured data from the hardware, we were even able to identify a wiring error that had been the source of the instability problem. The controller electronics were modified and, finally, the system was tuned up to full performance. The final system performance was demonstrated to be very robust and quite insensitive to physical changes in the plant or component values in the control electronics.

7. IN-FLIGHT PERFORMANCE

The in-flight performance of the system is shown by Figures 12 and 13. These figures were constructed with digitized data from the displacement transducers in one axis and serve to illustrate the performance of both axes. Since the accuracy of the displacement transducers is better than the image degradation due to seeing, tracking accuracy, and optical imperfections, these data are a better measure of mechanical performance of the system than chopped star images taken through the telescope.

These data were taken with the secondary mirror chopping in azimuth, such that both actuator axes were moving with the sample amplitude and in phase with each other. The chop amplitude (in sky-angle) that is indicated at the top of the plots is the total angle. The sky-angle that corresponds to each axis is 70 percent of this. Data is shown at two frequencies (10, 30 Hz) and an amplitude (8 arcmin) that somewhat exceeds that which has been routinely used on the KAO with earlier, more primitive secondary mirror systems. Unlike these earlier designs that had been used on the KAO, the new system shows no resonances at any particular functional frequencies or amplitudes, so the data are representative of the capability of the system over its entire design range.

Figure 12 is a greatly expanded view of a 70% x 8 arcmin = 340 arcsec, 10 Hz waveform. This figure shows that while there is a very small overshoot (on order of 2 to 3 arcsec) at each end of the chop, the waveform is stable from chop to chop at a level of about 0.5 arcsec. This overshoot decreases in proportion to the chop amplitude. The chop stability is a matter of some concern since the lightweight mirror is suspended just below the boundary layer of the 400 knot airflow past the open telescope cavity. There is no evidence that telescope vibration or wind shake affects the chop profile.

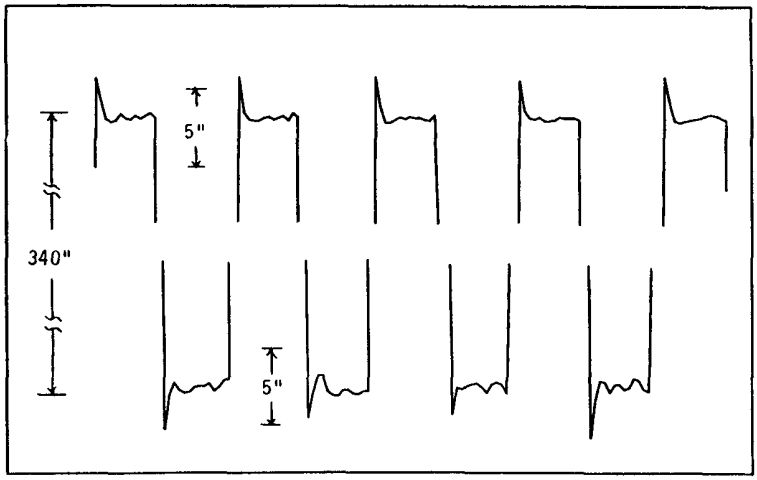

Fig. 12. Expanded scale of chopping motion in X-axis for 8 arcmin (sky-angle) and 10 Hz chop rate.

Figure 13(a & b) shows the component of the image point source profile that is due to the X-axis chopper at 10 and 30 Hz, respectively. The histograms have been produced with one arcsec (sky-plane) binning. The sharp spikes at each end of the plot are the two images produced by the chopper. Inset in each plot is a magnified view of these images. A total of 2,048 samples were taken for each data set, so the efficiency with which the system puts the image power into a 1 arcsec spot at the focal plane is seen to be about 80 percent and 54 percent for 10 Hz and 30 Hz, respectively, where a perfect square wave chop is 100 percent. Within a "seeing" limited spot size of ~4 arcsec, the efficiency rises to 88 percent and 70 percent, respectively. Evidence for a small amount of overshoot can be seen in these histograms.

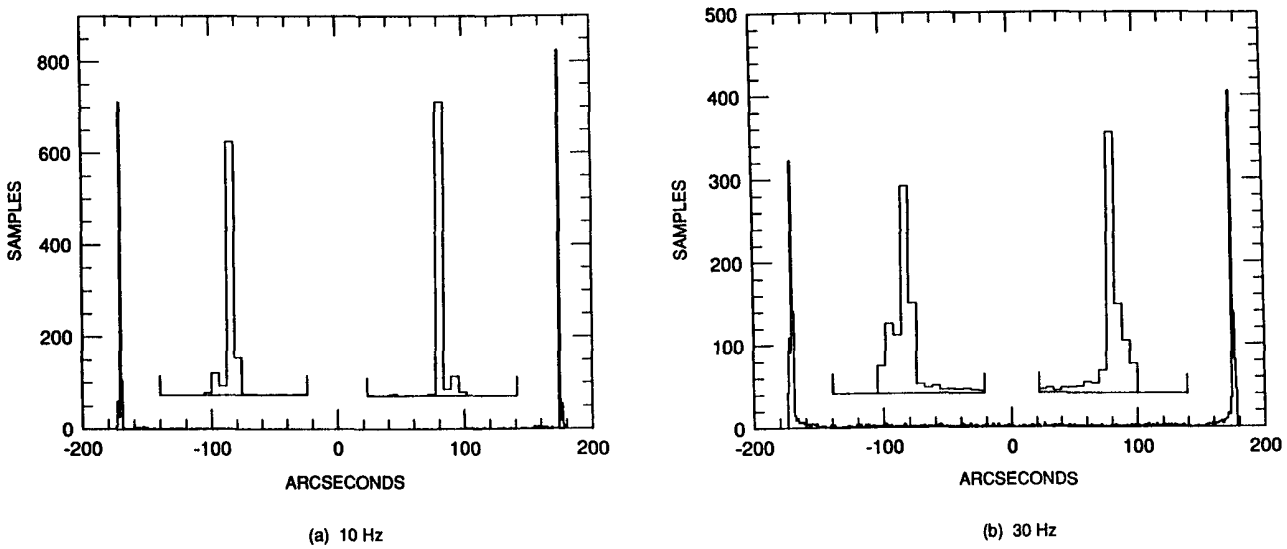

Fig. 13. Histograms of chopping motion for 8 arcmin (sky-angle) and two chop rates with 1 arcsec bin size.